GP96 drives exacerbation of secondary bacterial pneumonia following influenza A virus infection

Tomoko Sumitomo[1*], Masanobu Nakata[1, 2], Satoshi Nagase[3], Yuki Takahara[1], Mariko Honda-Ogawa[1], Yasushi Mori[1], Masaya Yamaguchi[1], Shigefumi Okamoto[3], Shigetada Kawabata[1*]

[1]Department of Oral and Molecular Microbiology, Osaka University Graduate School of Dentistry, Osaka, Japan

[2]Department of Oral Microbiology, Kagoshima University Graduate School of Medical and Dental Sciences, Kagoshima, Japan

[3]Department of Clinical Laboratory Science, Faculty of Health Sciences, Institute of Medical Pharmaceutical and Health Sciences, Kanazawa University, Kanazawa, Japan

*Corresponding authors: Tomoko Sumitomo, sumitomo@dent.osaka-u.ac.jp; Shigetada Kawabata, kawabata@dent.osaka-u.ac.jp.

Keywords: *Streptococcus pneumoniae*, influenza virus, superinfection, pneumonia

Abstract

Influenza A virus (IAV) infection predisposes the host to secondary bacterial pneumonia, known as a major cause of morbidity and mortality during influenza epidemics. Analysis of interactions between IAV-infected human epithelial cells and *Streptococcus pneumoniae* revealed that infected cells ectopically exhibited the endoplasmic reticulum chaperon GP96 on the surface. Importantly, efficient pneumococcal adherence to epithelial cells was imparted by interactions with extracellular GP96 and integrin α_V, with the surface expression mediated by GP96 chaperone activity. Furthermore, abrogation of adherence was gained by chemical inhibition or genetic knockout of GP96, as well as addition of RGD peptide. Direct binding of extracellular GP96 and pneumococci was shown to be mediated by pneumococcal oligopeptide permease components. Additionally, IAV infection induced activation of calpains and Snail1, which are responsible for degradation and transcriptional repression of junctional proteins in the host, respectively, indicating increased bacterial translocation across the epithelial barrier. Notably, treatment of IAV-infected mice with the GP96 inhibitor enhanced pneumococcal clearance from lung tissues and ameliorated lung pathology. Taken together, the present findings indicate a viral-bacterial synergy in relation to disease progression and suggest a paradigm for developing novel therapeutic strategies tailored to inhibit pneumococcal colonization in an IAV-infected respiratory tract.

Introduction

Secondary bacterial infection following influenza infection is associated with high rates of morbidity and mortality in elderly as well as chronically ill individuals. During the 1918 influenza pandemic, *Streptococcus pneumoniae* was identified as the predominant pathogen in more than 95% of all fatal cases[1]. Despite development of effective vaccines and potent antibacterial agents, during the 2009 H1N1 pandemic, bacterial pneumonia was a complication in one-quarter to one-half of severe and fatal cases[2]. The underlying mechanism of the viral-bacterial synergy leading to disease progression has remained elusive, thus hampering production of effective prophylactic and therapeutic intervention options.

Nasopharyngeal pneumococcal colonization is a major predisposing factor related to viral upper respiratory tract infections such as influenza[3, 4]. A preceding influenza virus infection can induce excess pneumococcal acquisition and carriage of the nasopharynx, which in turn promotes bacterial dissemination to the lungs. Although respiratory epithelium provides a physical barrier against most human pathogens, the influenza virus prefers to replicate in epithelial cells, leading to direct damage of airway epithelium[5, 6]. Virus-induced epithelial damage and exfoliation provide increased receptor availability for bacteria, resulting in establishment of bacterial colonization and onset of invasive diseases. For example, the influenza virus neuraminidase cleaves sialic acid glycoconjugates on airway epithelial cells as well as mucins, which facilitates

not only bacterial adherence to cryptic receptors but also their proliferation in the upper respiratory tract[7]. Among bacterial receptors appearing on cell surfaces during influenza infection, platelet-activating factor receptor (PAFR) gained attention as a possible therapeutic target[8]. Extracellular PAFR binds to phosphorylcholine embedded in the cell walls of numerous respiratory bacterial pathogens, which subsequently accelerates lung bacterial burden and bacteremia, and increases mortality risk. However, previous studies have found that genetic knockout or pharmacological inhibition of PAFR had no effect on susceptibility of mice to secondary bacterial pneumonia, implicating multifaceted mechanisms related to the synergism between influenza viruses and bacterial pathogens[9, 10].

A dual viral-bacterial infection causes dysfunction of the epithelial-endothelial barrier and, consequently, exudation of fluids, erythrocytes, and leukocytes into alveolar spaces, leading to gas exchange impairment and severe respiratory insufficiency. Indeed, pulmonary edema and hemorrhage are commonly found in autopsy examinations[1]. The physical barrier function of airway epithelium is provided by four types of cell-cell junctions; tight, adherens, and gap junctions, and desmosomes. Influenza virus-induced disruption of the pulmonary barrier is associated with a loss of integrity of claudin-4, a tight junctional protein[11]. Moreover, interaction between the PDZ-binding motif of the avian influenza virus NS1 protein and the PDZ domain present in tight junctional proteins has been shown to destabilize epithelial junctional integrity[12].

Although it is generally accepted that viral-induced epithelial cell damage allows for bacterial invasiveness, the molecular mechanisms involved in dysfunction of the alveolar epithelial barrier followed by bacterial dissemination remain largely unknown.

In the present study, novel findings showing that glycoprotein 96 (GP96), a host chaperone protein, is involved in exacerbation of bacterial pneumonia following influenza A virus (IAV) infection are presented. Interactions of pneumococci with extracellular GP96 and integrins, whose surface expressions are mediated by the chaperone activity of GP96, were found to promote pneumococcal adherence to IAV-infected epithelial cells. Also, inhibition of GP96 rendered IAV-infected cells as well as tested mice less susceptible to *S. pneumoniae* infection. Accordingly, GP96 is considered to be a potential target for therapeutic strategies for treating patients with superinfection. Furthermore, to the best of our knowledge, the present results are the first to demonstrate that viral infection induces calpain/Snail1-dependent dysfunction of the pulmonary epithelial barrier, thus providing a route for secondary bacterial translocation into deeper tissues via paracellular junctions. Together, these findings suggest an underlying mechanism responsible for polymicrobial synergy in cases of secondary bacterial pneumonia.

Results

Influenza A virus infection induces surface display of GP96 on alveolar epithelial cells

Host inflammatory response to a viral infection leads to increased or ectopic expressions of multiple proteins that serve as host receptors for bacteria. As a first step toward understanding the pathogenesis of bacterial pneumonia following influenza, we attempted to determine which proteins were exposed on the surface of alveolar epithelial cells following viral infection. Human A549 alveolar epithelial cells were infected with influenza A virus (IAV), followed by exposure to a membrane-impermeable biotinylation reagent. Cell surface proteins were then obtained using streptavidin beads, and subjected to SDS-PAGE and silver staining, which showed several different upregulated proteins on the surfaces of IAV-infected epithelial cells (Fig. 1a, arrows). Mass spectrometry analysis of these proteins revealed peptides corresponding to an endoplasmic reticulum protein, components of intermediate filaments, a glycolytic protein, and an oxidative stress-related protein. Among the host molecules, we focused on the human endoplasmic reticulum (ER) chaperon GP96, also referred to as GRP94 or endoplasmin, in further examinations. Although GP96 has been found to be mainly localized in the ER, abundant evidence presented indicates that it is also exposed on the surface of different cell types under particular conditions, such as infection, cell activation, and necrotic cell death[13]. Surface-displayed GP96 is frequently exploited as a receptor for bacterial pathogens, including *Listeria monocytogenes*[14] and

Neisseria gonorrhoeae[15]. To examine whether exposed GP96 serves as a receptor for *S. pneumoniae*, bacterial adherence to the apical surface of epithelial cells infected with or without IAV was examined. *S. pneumoniae* showed more efficient adherence to IAV-infected as compared to non-infected cells, while the enhanced bacterial association was reduced by pretreatment with either a pharmacological inhibitor of GP96 (Fig. 1b) or anti-GP96 antibody (Fig. 1c). On the other hand, a preceding IAV infection had no effect on the ability of *S. pneumoniae* to adhere to GP96 knockout cells (Fig. 1d), indicating it to be a critical factor for bacterial colonization on IAV-infected alveolar epithelial cells. To visualize GP96 distribution and pneumococci, non-permeabilized cells were stained with anti-GP96 and anti-pneumococcal capsule antibodies, respectively (Fig. 1e). GP96 was poorly visualized on the surface of non-infected cells, whereas its surface expression was markedly increased in response to IAV infection. Notably, co-localization of pneumococci with GP96 was observed in superinfected cells. Based on these results, we speculated that redistribution of GP96 on epithelial surfaces caused by IAV infection has a crucial role in secondary bacterial colonization in the lungs.

Pneumococcal surface proteins AliA and AliB are determinants of bacterial adherence via GP96 receptor

In the early stage of infection, bacterial pathogens secrete a variety of virulence factors that interact with host receptors for establishment of colonization. To identify bacterial factors responsible for GP96-mediated adherence to IAV-infected epithelial cells, pneumococcal cell wall fractions were obtained and reacted with recombinant GP96 protein, then GP96-binding proteins were recovered by immunoprecipitation with an antibody against GP96. As shown in Figure 2a, protein bands with an apparent molecular mass of approximately 70 kDa were identified as AliA and AliB by mass spectrometry analysis. AliA and AliB are components of oligopeptide permease, and have functions related to bacterial colonization in the pharynx and lung[16]. To examine the interactions of each with GP96, immobilized recombinant Ali proteins and the predominant pneumococcal surface protein PhtD, used as a control, were incubated with serially diluted GP96, followed by detection with an anti-GP96 antibody. GP96 was found to bind to the AliA and AliB proteins, but not to PhtD (Fig. 2b). Furthermore, the binding affinity of Ali proteins to GP96 was evaluated using surface plasmon resonance (SPR) measurements. Equilibrium dissociation constants for the binding of AliA and AliB to GP96 protein were calculated by applying association and dissociation curves to a 1:1 Langmuir binding model (Table 1). SPR analysis revealed that both AliA and AliB bound to GP96 with a high affinity, with K_D values of 3.40×10^{-8} and 4.85×10^{-8} M, respectively. We next examined whether these pneumococcal Ali proteins function as adhesins for bacterial adherence to IAV-infected epithelial cells. Following IAV

infection, the association of a wild-type (WT) strain to alveolar epithelial cells was increased by approximately 2.5-fold, whereas the adhesion activity of the *aliA* and *aliB* mutants remained unchanged (Fig. 2c). These results suggest that *S. pneumoniae* utilizes AliA and AliB proteins as adhesins to interact with surface-displayed GP96 on IAV-infected cells, resulting in establishment of a secondary pneumococcal infection.

Influenza infection-induced chaperoning activity of GP96 promotes pneumococcal adherence to alveolar epithelial cells

GP96 is a molecular chaperone that has a key role in folding as well as surface expression of various integrin subunits and Toll-like receptors (TLRs)[17]. Integrins are type I transmembrane heterodimeric proteins that mediate cell-cell and cell-extracellular matrix interactions. The major integrin ligand fibronectin (Fn) possesses a tripeptide arginine-glycine-aspartic acid (RGD) sequence that serves as the integrin recognition site. Bacterial pathogens responsible for secondary bacterial pneumonia, including *S. pneumoniae*, *Streptococcus pyogenes*, *Staphylococcus aureus*, and *Haemophilus influenzae*, utilize interactions with Fn-integrins to associate with host cells[18-21]. Thus, we speculated that IAV infection accelerates a GP96-dependent surface display of integrins that may augment bacterial association with epithelial cells. To examine in more detail, immunoprecipitation of cell lysates containing biotinylated surface

160 proteins extracted from non-infected and IAV-infected epithelial cells was conducted using an
161 antibody against integrin α_V, a major α subunit involved in the pathogenesis of respiratory
162 diseases. The expression levels of total integrin α_V were similar among all tested conditions,
163 whereas a slight shift of the protein band potentially reflecting modification of sugar moiety was
164 observed in IAV-infected cells (Fig. 3a, right panel). Notably, a marked increase in surface-
165 exposed integrin α_V was seen following IAV infection, which was largely abrogated by
166 introduction of the GP96 inhibitor, suggesting that integrin α_V is exported to the surface of IAV-
167 infected cells in a GP96-dependent manner (Fig. 3a, left panel). Immunofluorescence staining
168 experiments also revealed that co-localization of integrin α_V with GP96 on the cell surface was
169 more pronounced with IAV infection (Fig. 3b).

170 Next, we evaluated whether surface-exposed integrin α_V functions as a receptor for bacterial
171 adherence to IAV-infected cells. As shown in Figure 3c, *S. pneumoniae* demonstrated a greater
172 level of adherence to IAV-infected as compared to non-infected cells, though that enhanced
173 bacterial association was partially reduced by treatment with an anti-integrin α_V antibody.
174 Furthermore, as compared with a control peptide, an RGD-containing peptide abrogated
175 pneumococcal adhesion in a dose-dependent manner (Fig. 3d). Thus, Fn-integrin interaction was
176 also found to be associated with pneumococcal adherence to IAV-infected alveolar epithelial cells.
177 We considered that the increased level of pneumococcal adherence to IAV-infected cells in the

178 presence of control peptide was likely due to *S. pneumoniae* utilizing the synthetic peptides as a
179 nutrient source. Together, these results provide evidence that IAV infection enhances the surface
180 expression of integrin α_V through the chaperone activity of GP96, thereby increasing
181 pneumococcal adherence to alveolar epithelial cells.
182
183 **Influenza infection-induced Snail1 expression contributes to disruption of alveolar epithelial**
184 **barrier**
185 Calcium (Ca^{2+}) signaling has been implicated to be involved in various stages of host-pathogen
186 interactions during viral and bacterial infections. Indeed, previous studies have shown that IAV
187 infection induces Ca^{2+} influx, then elevated intracellular Ca^{2+} promotes endocytic uptake of the
188 virus and host inflammatory response[22, 23]. Also, Ca^{2+} influxes activate calpains, Ca^{2+}-dependent
189 host cysteine proteases, which then target junctional proteins, such as occludin and E-cadherin[24].
190 Since calpains have been shown to change their distribution in an active state[25], cellular
191 localization of GP96 and calpains in IAV-infected alveolar epithelial cells was assessed using
192 immunofluorescence staining. As opposed to GP96, calpain 2 was not only exposed on the apical
193 surface of epithelial cells but also found concentrated in the plasma membrane region after IAV
194 infection (Fig. 4a). Our observations suggest that IAV infection recruits calpains to the plasma
195 membrane of paracellular junctions, which in turn promotes destabilization of the alveolar

196 epithelial barrier through degradation of junctional proteins. We then evaluated the effects of IAV
197 infection on expressions of GP96 and calpains, as well as junctional proteins associated with
198 epithelial barrier function using quantitative RT-PCR analysis. Distinct downregulation of E-
199 cadherin and p120-catenin was detected in IAV-infected cells, whereas that infection had no effect
200 on expression of GP96 or calpains at the transcriptional level (Fig. 4b). These results imply that
201 IAV infection does not induce increased expression levels of GP96 and calpains, but rather results
202 in their ectopic localization in epithelial cells.

203 Interestingly, IAV infection induced a drastic upregulation of the host transcriptional factor
204 Snail1, a global repressor of genes encoding junctional proteins[26, 27]. TGF-β has been shown to
205 downregulate the expression of E-cadherin via the snail signaling pathway, known to be
206 fundamental for development of epithelial-to-mesenchymal transition (EMT)[28]. To investigate the
207 association of Snail1 expression with destabilization of junctional proteins following infection,
208 alveolar epithelial cells were infected with IAV in the presence or absence of a TGF-β inhibitor,
209 then subsequently infected with *S. pneumoniae* (Fig. 4c). The protein level of Snail1 was elevated
210 during both IAV infection and superinfection, whereas inhibition of the TGF-β pathway by SB-
211 431542 in the co-infected cells resulted in remarkably reduced Snail1 levels in a dose-dependent
212 manner. Along with increased levels of Snail1, reduced expression levels of E-cadherin and p120-
213 catenin were observed in both IAV- and co-infected cells, while those were completely restored

214 in the presence of the TGF-β inhibitor. Together, these data suggest that IAV infection induces
215 Snail1-dependent dysfunction of the alveolar epithelial barrier via the TGF-β signaling pathway,
216 thus providing a route for secondary pneumococcal dissemination.
217
218 **GP96 involved in exacerbation of bacterial pneumonia following influenza infection**
219 To further clarify the role of IAV-induced GP96 in secondary pneumococcal pneumonia *in vivo*,
220 mice were intranasally infected with a nonlethal dose of IAV (day 0), which was followed by
221 intratracheal administration of the vehicle or GP96 inhibitor PU-WS13 on day 5, then intranasal
222 challenge with *S. pneumoniae* was done on day 6 (Fig. 5a). At two days after bacterial infection,
223 co-infected mice showed a significantly greater bacterial burden in the lungs as compared to those
224 infected with *S. pneumoniae* only (Fig. 5b). Notably, PU-WS13 treatment resulted in a remarkable
225 reduction in bacterial colonization in the lungs of the co-infected mice (Fig. 5b), indicating that
226 mediation of GP96 induction by IAV infection has a key role in the pathogenesis of secondary
227 bacterial pneumonia *in vivo*. Among integrin subsets, integrin $\alpha_V\beta_6$ is an epithelium-restricted
228 molecule expressed at low levels in the lungs of healthy individuals, then becomes rapidly
229 upregulated in response to inflammation and injury. Meliopoulos, *et al.* reported that integrin β_6
230 is an important factor associated with the severity of influenza diseases[29]. To further elucidate the
231 mechanism by which IAV infection leads to increased susceptibility to secondary bacterial

232 pneumonia, we examined the expression levels of integrin β_6 and GP96 in pharyngeal and lung
233 tissues at one day after bacterial administration under each infection condition (Fig. 5c, d).
234 Quantitative RT-PCR analysis showed that IAV infection resulted in an approximately two-fold
235 increase in expression levels of GP96 and integrin β_6 in pharyngeal tissues (Fig. 5c), but not in
236 lung tissues (Fig. 5d). Of note, high expression levels of GP96 and integrin β_6 were detected in
237 both pharyngeal and lung tissues after superinfection. These results suggest that pneumococcal
238 colonization in the IAV-infected upper respiratory tract triggers GP96 expression in lung tissues,
239 which in turn allows bacterial dissemination to the lower respiratory tract. Histopathological
240 analysis was also performed using lungs obtained from mice at two days after pneumococcal
241 infection (Fig. 5e). In lung tissues infected with IAV alone, moderate levels of inflammatory cell
242 infiltration in peribronchiolar and interalveolar spaces, as well as microvascular hemorrhage were
243 observed. Mice infected with *S. pneumoniae* alone also showed prominent perivascular and
244 peribronchiolar lymphocytic cuffing. In contrast, mice with co-infection demonstrated dense
245 leukocytic infiltration in interstitial and alveolar spaces, along with hemorrhaging, vascular
246 leakage, and edema formation, suggesting vascular damage and increased epithelial-endothelial
247 permeability. Notably, PU-WS13 treatment resulted in improvement of lung pathology in co-
248 infected mice. To investigate lung tissue integrity in superinfected mice, we examined the
249 expression of E-cadherin in lung tissues obtained from IAV- as well as co-infected mice. Those

250 with co-infection exhibited a marked decrease in E-cadherin expression as compared to mice
251 infected with IAV alone, while that was partially restored by PU-WS13 treatment (Fig. 5f). Taken
252 together, our results indicate that GP96 is a factor for exacerbation of secondary bacterial
253 pneumonia following influenza as well as a promising novel target for therapeutic intervention.

Discussion

Secondary bacterial infections following a primary influenza virus infection are frequent complications, and result in the majority of related deaths during seasonal and pandemic influenza outbreaks. *S. pneumoniae* is the most commonly identified pathogen in secondary bacterial pneumonia cases. Although antibiotics remain the mainstay of therapy for affected patients, the increasing prevalence of multidrug-resistant *S. pneumoniae* is a serious public health concern worldwide. Thus, development of host-directed therapeutics is receiving focus as an alternative approach to treating secondary bacterial pneumonia following influenza. The present findings showed that GP96 functions as an exacerbation factor for secondary bacterial infections following influenza, thus we propose GP96 as a potential therapeutic target for novel countermeasures used to treat bacterial pneumonia.

GP96, an ER-resident HSP90 paralogue, has been reported to be exposed on the surface of various types of cells by multiple types of microbial infection[13]. The present is the first study to show that IAV infection triggers surface distribution of GP96 in human airway epithelial cells, where it is then hijacked as a host receptor for secondary infection by *S. pneumoniae*. The interaction between extracellular GP96 and bacterial surface ligands has been shown to activate host signaling cascades that facilitate bacterial adherence and internalization. Indeed, pathogenic *Escherichia coli* targets Ecgp96, a homologue of GP96 expressed on human brain microvascular

endothelial cells, induces rearrangement of actin microfilaments and disassembly of endothelial junctions through signaling-mediated Ca^{2+} influx and nitric oxide production, resulting in acceleration of bacterial invasion[30, 31]. Bacterial pore-forming toxins such as pneumolysin produced by *S. pneumoniae* also induce similar cellular events in host cells[32]. Although the present results demonstrated that IAV infection induces Ca^{2+}-dependent calpain activation, which then evokes destabilization of paracellular junctions without bacterial infection, *S. pneumoniae* may utilize not only extracellular GP96-mediated signaling but also pneumolysin-induced cell damage for invasion into deeper tissues. Despite increased understanding regarding the roles of GP96 in the pathogenesis of infections, the molecular mechanisms underlying surface distribution remain unidentified. Recently, plasma membrane damage mediated by bacterial pore-forming toxins was shown to be associated with redistribution of GP96 via non-muscle myosin II activity and Ca^{2+} influx during *Listeria monocytogenes* infection[33]. Although the mechanism governing the surface distribution of GP96 following IAV infection remains largely unknown, it is likely that calcium homeostasis and Ca^{2+}-dependent effectors have key roles in IAV-infected airway epithelial cells.

Bacterial colonization in the upper respiratory tract is considered to be a prerequisite for invasive infection, which results in bacterial invasion into other tissues or dissemination to the lower respiratory tract. In addition to a drastic increase in receptor availability accompanied by influenza virus infection, *S. pneumoniae* also possesses a variety of adhesins that augment bacterial

290 adherence to these newly exposed receptors[34]. Herein, we identified AliA and AliB as bacterial
291 adhesins for the display of GP96 on the surface of alveolar epithelial cells following IAV infection.
292 These oligopeptide-binding proteins are conserved among bacterial pathogens most frequently
293 associated with influenza, including *S. pneumoniae*, *S. pyogenes*, *S. aureus*, and *H. influenza*.
294 GP96 serves as the host cellular receptor for various bacterial adhesins, such as pathogenic *E. coli*
295 OmpA[30, 31], *L. monocytogenes* Vip[14], *S. aureus* Bap[35], and *Clostridium difficile* enterotoxin A[36],
296 though those proteins share no homology with Ali proteins. Since GP96 might nonspecifically
297 interact with multiple bacterial molecules on account of its chaperone structure, bacterial
298 pathogens likely utilize ectopically exposed GP96 for establishment of bacterial colonization.
299 Transforming growth factor (TGF-β), a multifunctional cytokine, is secreted in an inactive or
300 latent form, then subsequently activated through various mechanisms. During IAV infection, viral
301 neuraminidase was shown to activate TGF-β, which promoted upregulation of host adhesion
302 molecules, including fibronectin and integrins[37]. TGF-β is also a positive regulator of the integrin
303 signaling pathway that promotes cytoskeletal rearrangement and bacterial internalization[38].
304 Indeed, we previously reported that *S. pyogenes* possesses Fn-binding molecules and utilizes Fn-
305 integrin interactions to adhere to and invade IAV-infected cells[39]. In addition to TGF-β signaling,
306 the present findings showed that IAV infection induces upregulation and display of integrins on
307 the surface of alveolar epithelial cells via a chaperoning activity of GP96. Furthermore, GP96

serves as an essential chaperon for the cell-surface protein glycoprotein A repetitions predominant (GARP), a docking receptor for latent membrane-associated TGF-β[40], indicating GP96 as a crucial factor for TGF-β signaling. Notably, *S. pneumoniae* also expresses neuraminidases on bacterial cell walls. NanA, a primary pneumococcal neuraminidase, is a sialidase that catalyzes cleavage of terminal sialic acids from latency-associated peptide (LAP) and also activates TGF-β signaling[41]. Another study showed that activation of TGF-β signaling proceeds through phosphorylation of SMAD proteins, which is associated with Snail1-mediated down-regulation of tight junction proteins of epithelial and endothelial cells[42]. The present results provide evidence that a preceding influenza infection induces a Snail1-dependent dysfunction of the airway epithelial barrier through TGF-β signaling, thus preparing a route for secondary pneumococcal translocation into deeper tissues via paracellular junctions. Therefore, the synergistic effects of the GP96 chaperoning function and viral-pneumococcal neuraminidase activities likely prime potent TGF-β signaling, which leads to increased bacterial loading in the lungs and pulmonary barrier dysfunction.

Besides being exploited as a host receptor for variety of pathogens, GP96 modulates host immune response to counteract an infection. GP96 functions as a master chaperone for cellular localization and function of TLRs. During an influenza infection, TLRs act as key transducers of type I interferons (IFNs) by recognition of viral nucleic acid[4]. It is known that type I IFN signaling

326 through the IFN-α/β receptor evokes expression of proinflammatory genes to inhibit viral
327 replication and augment various aspects of adaptive immunity, while several lines of evidence
328 also indicate that neutrophil function is impaired following influenza virus infection. Viral
329 infection-primed expression of type I IFNs is sufficient to interfere with production of specific
330 chemokines, such as CXCL1 and CXCL2, resulting in impairment of neutrophil response during
331 secondary *S. pneumoniae* infection[43]. The present findings showed that pneumococcal
332 colonization in the upper respiratory tract triggered upregulation of GP96 in murine pharyngeal
333 and lung tissues infected with IAV through an unidentified mechanism. Accordingly, given the
334 importance of GP96 in TLRs signaling[17], IAV infection-induced GP96 might impair immune
335 responses against *S. pneumoniae* by excess production of type I IFNs. On the other hand, GP96
336 has been shown to specifically bind to and activate neutrophils and monocytes[44]. Nevertheless,
337 we speculate that binding of pneumococcal Ali proteins to GP96 interferes with direct interactions
338 of GP96 with neutrophils as well as monocytes in cases of viral-bacterial dual infection. Although
339 direct evidence showing that GP96 is related to impairment in macrophages and neutrophil
340 responses following IAV infection remains lacking, it may function as a potent receptor for
341 bacterial colonization as well as an immune regulator in dysfunction of innate immune defenses
342 against bacterial infection.

343 Taken together, the present results indicate that GP96 functions as a multifunctional exacerbation
344 factor to promote pneumococcal colonization dysfunction of lung tissue, barrier, and probably
345 dysregulation of immune responses as well, during secondary bacterial pneumonia following an
346 influenza infection. Because of the complexity of the pathogenesis, a balanced combination of
347 antimicrobial agents and immunomodulators could be more effective for prospective therapeutics.
348 We believe that GP96 is a potential target for development of promising therapeutic strategies,
349 including combination therapies as alternatives to conventional antibiotics and antiviral agents
350 administered for broad-spectrum prevention, as well as management of secondary bacterial
351 infections following influenza.

352

353

354 **Methods**

355 **Bacterial and viral strains and culture conditions**

356 *Streptococcus pneumoniae* D39 (serotype 2 clinical isolate) and isogenic mutant strains were
357 cultured in Todd-Hewitt broth (Becton, Dickinson and Company; BD) supplemented with 0.2%
358 yeast extract (BD) (THY medium) at 37ºC in an ambient atmosphere. For selection and
359 maintenance of mutant strains, spectinomycin (Sigma-Aldrich) at 100 μg/ml was added to the
360 medium. *Escherichia coli* strains BL21-gold (DE3) (Agilent Technologies) and XL10-gold
361 (Stratagene) served as hosts for derivatives of plasmids pGEX-6P-1 (Cytiva) and pQE30 (Qiagen),
362 respectively. All *E. coli* strains were cultured in Luria-Bertani (Nacalai Tesque) (LB) medium at
363 37ºC with agitation. For selection and maintenance of *E. coli* mutant strains, ampicillin (100
364 μg/ml) was added to the medium. Influenza A virus A/FM/1/47 (H1N1) was grown in Madin-
365 Darby canine kidney (MDCK) cells.

366

367 **Cell cultures and construction of GP96 knockout cells**

368 The human alveolar carcinoma cell line A549 (Riken Cell Bank) derived from type II
369 pneumocytes and MDCK were maintained in DMEM supplemented with 10% FBS at 37ºC under
370 a 5% CO_2 atmosphere.

371 A CRISPR-Cas9 GP96 knockout plasmid was created by cloning sgRNA GP96 oligos into a

372 pSpCas9(BB)-2A-Puro (PX459) plasmid, a gift from Feng Zhang (Addgene plasmid #62988)[45].
373 The constructed plasmid was then transfected into A549 cells with Lipofectamine 3000 Reagent
374 (Thermo Scientific), according to the manufacturer's instructions. At 24 hours after transfection,
375 1.5 μg/ml puromycin was added and the cells were further cultured for two days. Next, a limiting
376 dilution of the survived cells was conducted and single colonies were expanded, with GP96
377 expression examined by Western blot analysis using anti-Grp94 rabbit Ab (Cell Signalling). PCR
378 products were amplified with purified genomic DNA, and the primers gp96checkF and
379 gp96checkR, then subjected to Sanger sequencing for confirmation of mutations. All primers used
380 are listed in Supplementary Table 1.
381
382 **Preparation of *S. pneumoniae* mutant strains and recombinant proteins**
383 Inactivation of the *aliA* and *aliB* genes was achieved by transformation of strain D39 with a
384 linear DNA fragment containing a spectinomycin resistance gene (*aad9*) flanked by the upstream
385 and downstream sequences of the *aliA* and *aliB* genes, as previously reported[46].
386 For construction of recombinant GP96, cDNA of A549 cells was prepared using Trizol and a
387 PureLink RNA mini-kit (Thermo Scientific). cDNA fragments encoding full-length GP96 were
388 amplified using specific primers (Supplementary Table 1). The fragments were cloned into a
389 pGEX-6P-1 vector via the *BamH*I and *Sal*I sites, then transformed into *E. coli* BL21 (DE3).

Recombinant AliA and AliB proteins were hyper-expressed in *E. coli* XL10-Gold using a pQE30 vector. N-terminal His-tagged proteins were purified using a QIAexpress protein purification system (Qiagen), as previously described[47].

Adherence assay.

A549 cells were cultured in 24-well plates at a density of 2 x 10^5 cells per well and infected with 10^6 PFU of IAV in serum-free DMEM supplemented with 0.1% BSA (Sigma-Aldrich), MEM vitamin solution (Thermo Scientific), and 0.01% DEAE dextran (GIBCO) for one hour at 34ºC. Following washing steps, the cells were incubated for 36 hours in the presence or absence of PU-WS13 (Merck Millipore). *S. pneumoniae* strains were grown to the exponential phase (OD_{600} = 0.7), then washed with and resuspended in PBS. IAV-infected cells were exposed to 10^7 CFU of pneumococci in DMEM supplemented with 10% FBS for two hours at 37ºC. For quantification of bacterial adherence, infected cells were washed with PBS and lysed with distilled water. Serial dilutions of the lysates were plated on THY agar plates to determine CFU.

In some experiments, antibodies targeting Grp94 (Rat, mAb, Enzo) and integrin α_V (Goat, pAb, R&D), rat IgG2A isotype control (Rat, mAb, R&D), normal goat IgG control (Goat, pAb, Enzo), RGD peptide (Gly-Arg-Gly-Asp-Asn-Pro, Enzo), and RGD control peptide (Gly-Arg-Ala-Asp-Ser-Pro, Enzo) were added to A549 cells at one hour before infection with *S. pneumoniae*.

Immunoprecipitation assay.

Cell surface proteins were biotinylated using an EZ-Link Sulfo-NHS-Biotin reagent (Thermo Scientific) following the manufacturer's protocol. Briefly, non-infected and IAV-infected A549 cells were washed with PBS, then incubated with 1 mM Sulfo-NHS-biotin for 30 minutes at room temperature. After quenching the biotin reagent with 100 mM glycine in PBS, the cells were lysed using radioimmunoprecipitation buffer containing Complete protease inhibitor (Roche Life Science) for 20 minutes at 4ºC. Cell surface proteins were precipitated with Dynabeads M-280 Streptavidin (Thermo Scientific), separated using SDS-PAGE, then visualized by silver staining. Bands of interest were analyzed by liquid chromatography-tandem mass spectrometry using a Q-Exactive Mass Spectrometer (Thermo Scientific) equipped with an UltiMate 3000 Nano LC System (Thermo Scientific). Raw data were processed using Mascot Distiller v2.5 (Matrix Science). Peptide and protein identification was performed with Mascot, v.2.5 (Matrix Science), using the UniProt database with a precursor mass tolerance of 10 ppm, a fragment ion mass tolerance of 0.01 Da, and strict trypsin specificity that allowed one missed cleavage. To determine cellular localization of integrin α_V, immunoprecipitation using an antibody against integrin α_V (Rabbit, pAb, Cell signaling) and Dynabeads Protein A (Thermo Scientific) was performed, then detection was done by Western blot analysis with a specific antibody against integrin α_V (Goat,

pAb, R&D) and a horseradish peroxidase (HRP)-conjugated antibody against goat IgG (R&D), or HRP-conjugated streptavidin (Thermo Scientific). Immunoreactive bands were detected using Pierce Western blotting substrate (Thermo Scientific).

For identification of bacterial factors associated with GP96, cell wall fractions of *S. pneumoniae* were prepared as previously described[49]. The fractions were incubated with 10 μg of recombinant GP96 for six hours at 4ºC. Proteins bound to GP96 were immunoprecipitated with an antibody against Grp94 (Rat, mAb, Enzo) and Dynabeads Protein G (Thermo Scientific), then examined using mass spectrometry analysis, as described above.

Surface plasmon resonance analysis

Association and dissociation reactions of GP96 to pneumococcal Ali proteins were analyzed using a BIAcore optical biosensor (BIAcore X-100 system, GE Healthcare Life Sciences), as previously described[48]. Briefly, recombinant GP96 (20 μg ml^{-1} in 10 mM sodium acetate, pH 4) was covalently immobilized on a CM5 sensor chip using an Amine coupling kit (GE Healthcare Life Sciences). Binding analyses were performed in HBS-P buffer (0.01 M HEPES, pH 7.4, 0.15 M NaCl, 0.005% surfactant P20; GE Healthcare Life Sciences) at 37ºC with a flow rate of 30 μl/min. AliA and AliB were separately used as an analyte at concentrations of 31.3, 62.5, 125, 250, and 500 nM. Parameters of binding kinetics were analyzed using raw data from the BIAcore

444 sensorgram suitable for analysis with the kinetic models included in the BIA evaluation software
445 package, v. 3.0.2 (GE Healthcare Life Sciences). Data were fitted using a 1:1 Langmuir binding
446 model.
447
448 **ELISA**
449 GP96 binding to AliA and AliB proteins was assessed by ELISA, as previously described[50].
450 Microtiter plates (96-well; Sumitomo Bakelite) were separately coated with AliA, AliB, and PhtD
451 protein (250 ng) in coating buffer (0.1 M Na_2CO_3, 0.1 M $NaHCO_3$, pH 9.6) at 4ºC overnight. The
452 plates were blocked with 10% Block Ace solution (Megmilk Snow Brand) at 4ºC overnight, then
453 washed with PBS containing 0.2% Tween 20 (PBST). GP96 was diluted with binding buffer (50
454 mM HEPES, pH 7.4, 150 mM NaCl, 2 mM $CaCl_2$, 50 μg/ml BSA) and incubated with
455 immobilized bacterial surface proteins for 90 minutes at 37ºC. After washing with PBST, the
456 plates were incubated with an antibody against GP96 (Sheep, pAb, R&D) for two hours at room
457 temperature. Subsequently, an HRP-conjugated antibody against sheep IgG (R&D) was added to
458 the plate and incubation was continued for two hours at room temperature. Following a washing
459 step, the peroxidase substrate tetramethylbenzidine (Moss) was added to the plate. The reaction
460 was stopped by addition of 0.5 N HCl and absorbance at 450 nm was measured using a Muktiskan
461 FC microplate photometer (Thermo Scientific).

462

463 **Immunofluorescence microscopy**

464 A549 cells were seeded at 2×10^5 onto cover slides (13-mm diameter; Matsunami) pretreated
465 with coating buffer containing 0.1% collagen (Type I from rat tail; Sigma-Aldrich) and 0.1%
466 gelatin (from bovine bone; Wako). The cells were then infected with IAV followed by *S.*
467 *pneumoniae*, as described above, and fixed with 4% paraformaldehyde-PBS. Following blocking
468 with 5% bovine serum albumin-PBS, the cells were reacted with a primary antibody targeting
469 Grp94 (Rat, mAb, Enzo), Grp94 (Rabbit, pAb, Thermo Scientific), integrin α_V (Mouse, mAb,
470 R&D), Calpain 2 (Rabbit-pAb, Cell Signaling), or serotype 2 capsule (Rabbit, pAb, Denka
471 Seiken). After washing steps, incubation was performed with Alexa Fluor 594-conjugated anti-
472 rat IgG (Thermo Scientific), Alexa Fluor 594-conjugated anti-mouse IgG (Thermo Scientific),
473 Alexa Fluor 488-conjugated anti-mouse IgG (Thermo Scientific), or Alexa Fluor 488-conjugated
474 anti-rabbit IgG (Thermo Scientific). To observe the association of pneumococci with GP96,
475 imaging was performed using a Zeiss LSM 510 confocal microscope system, v. 3.2 (Carl Zeiss)
476 and analyzed with the LSM 510 software package. For assessment of cellular localization of GP96,
477 integrin α_V, and calpain 2, cover slides were enclosed with ProLong Gold Antifade Reagent with
478 DAPI (Thermo Scientific) and examined using a Carl Zeiss Axioplan 2 fluorescent microscope
479 system.

480

481 **Analysis of destabilization of epithelial junctions**

482 Whole cell lysates from coinfected epithelial cells were prepared as previously described[49].
483 Briefly, A549 cells were infected with IAV in the presence or absence of SB-431542, a TGF-β
484 inhibitor. At seven hours after infection, the cells were lysed with Laemmli gel loading buffer
485 containing 6% 2-mercaptoethanol. Cleavage of junctional proteins was detected by Western blot
486 analysis using specific antibodies against E-cadherin (Mouse, mAb, Thermo Scientific), p120-
487 catenin (Rabbit, pAb, Cell Signaling), Snail1 (Mouse, mAb, Cell Signaling), and β-actin (rabbit,
488 pAb, Cell Signaling). Horseradish peroxidase (HRP)-conjugated antibodies against mouse or
489 rabbit IgG (Cell Signaling) were used as the secondary antibodies.

490

491 **Mouse experiments.**

492 Female BALB/c mice at six to eight weeks old (CLEA Japan, Inc.) were intranasally infected
493 with 3.5 PFU of IAV A/FM/1/47 (H1N1) in 40 μl PBS (day 0). The *S. pneumoniae* D39 strain
494 was grown to the mid-exponential phase (OD_{600} = 0.4), then washed with and resuspended in PBS.
495 Bacteria were introduced into the mice by intranasal administration of 1×10^6 CFU in 40 μl PBS
496 on day six. In some experiments, mice were intratracheally treated with either the vehicle or PU-
497 WS13 (20 mg/kg mouse body weight) on day five.

For quantification of bacterial colonization in the lung, mice were euthanized two days after *S. pneumoniae* infection, then lung tissues were immediately collected. Lung homogenates were serially diluted and plated on THY agar plates containing 5% sheep blood. For histopathologic examinations, lung tissue samples were obtained and fixed with formalin, then embedded in paraffin and sectioned, and subjected to hematoxylin and eosin (HE) staining. Stained tissue sections were observed using an EVOS M5000 cell Imaging system (Thermo Scientific). For assessment of gene expression, pharyngeal and lung tissues were harvested at various time points.

Real-time RT-PCR assay

Total RNA was isolated from A549 cells using a CellAmp Direct RNA Prep Kit (TaKaRa), as well as murine pharyngeal and lung tissues using an RNeasy Fibrous Tissue Mini Kit (QIAGEN). Synthesis of cDNA from total RNA was performed with a PrimeScript RT reagent Kit (TaKaRa). The possibility of DNA contamination was excluded by PCR analysis of non-RT samples. Primer sets for selected genes were designed using Primer Express Software, version. 3.0 (Applied Biosystems). All primers used are listed in Supplementary Table 1. RT-PCR amplifications were performed using the SYBR Green method with an ABI StepOne™ Real-Time PCR System, v. 2.2 (Applied Biosystems). Relative expression amounts were calculated with the $\Delta\Delta C_T$ method. The level of *gapdh* expression was used as an internal control.

Statistical analysis.

All statistical analyses were performed using GraphPad Prism, v. 7.03 (GraphPad Software). Differences were determined with Mann-Whitney's *U* test when comparing two groups, or one-way ANOVA, followed by Tukey's multiple comparison test when comparing multiple groups. A confidence interval with a *P* value of <0.01 was considered to be significant.

Ethics statement.

All mouse experiments were conducted using a protocol approved by the Animal Care and Use Committee of Osaka University Graduate School of Dentistry (authorization number 01-010-0) and the Animal Care and Use Committee of Kanazawa University (authorization numbers AP-143262 and AP-183936).

528 **Figure legends**

529

530 **Fig. 1. IAV infection-induced surface display of GP96 promotes pneumococcal adherence.**

531 **a**, A549 cells were infected with 10^6 PFU of IAV for 36 hours, then treated with a membrane-
532 impermeable biotinylation regent. Cell surface proteins were obtained using streptavidin beads,
533 then subjected to SDS-PAGE and silver staining. Arrows indicate bands of upregulated surface
534 proteins after IAV infection. **b**, **c**, A549 cells were infected with IAV for one hour. Following
535 washing steps, they were incubated for 36 hours in the presence of PU-WS13 (**b**) or an antibody
536 against GP96 (**c**). Next, IAV-infected cells were coinfected with *S.pneumoniae* D39 strain at an
537 MOI of 5. At two hours after infection, cells were lysed and cell-associated bacteria were
538 recovered. Bacterial adherence rate was calculated as percent of the inoculum. All experiments
539 were performed in sextuplet with three technical repeats. Values are shown as the mean ± S.D. of
540 six wells from a representative experiment. **d**, Effect of GP96 knockout on pneumococcal
541 adherence. Bacterial association with IAV-infected cells was normalized to that with non-infected
542 cells. All experiments were performed in sextuplet with three technical repeats. Values are shown
543 as the mean ± S.D. of six wells from a representative experiment. **P* <0.01 (**b**-**d**). **e**, A549 cells
544 were infected with IAV followed by *S. pneumoniae* infection. GP96 was labeled with anti-GP96
545 and Alexa Fluor 594-conjugated antibodies (shown as red in images), while *S. pneumoniae* was

546 labeled with anti-serotype 2 capsule and Alexa Fluor 488-conjugated antibodies (shown as green
547 in images). Images were analyzed using a confocal laser scanning microscope. Values shown are
548 representative of at least three separate experiments.
549
550 **Fig. 2. *S. pneumoniae* adheres to alveolar epithelial cells through interaction of**
551 **pneumococcal surface proteins with GP96.**
552 **a**, Proteins bound to GP96 were immunoprecipitated from pneumococcal cell wall fractions,
553 then subjected to SDS-PAGE and silver staining. **b**, AliA, AliB, and PhtD, bacterial surface
554 proteins, were immobilized on microtiter plates, then increasing amounts of GP96 were added.
555 Bound GP96 was detected using an anti-GP96 antibody. All experiments were performed in
556 sextuplet with three technical repeats. Values are shown as the mean ± S.D. of six wells from a
557 representative experiment. *P <0.01. **c**, Effects of deletion of *aliA* and *aliB* on pneumococcal
558 adherence. Bacterial association with IAV-infected cells was normalized to that with non-infected
559 cells. All experiments were performed in sextuplet with three technical repeats. Values are shown
560 as the mean ± S.D. of six wells from a representative experiment. *P <0.01.
561
562 **Fig. 3. GP96-dependent surface display of integrin α_V associated with enhanced**
563 **pneumococcal adherence following IAV infection.**

564 **a**, A549 cells were infected with IAV for 36 hours in the presence or absence of PU-WS13, then
565 treated with a membrane-impermeable biotinylation reagent. Immunoprecipitation of cell lysates
566 containing biotinylated surface proteins was performed using an antibody against integrin α_V.
567 Surface-displayed and whole-cell integrin α_V was detected using streptavidin and an antibody
568 against integrin α_V, respectively. Red arrows indicate integrin α_V band. **b**, A549 cells were
569 infected with IAV for one hour. After transferring to fresh medium, incubation was continued for
570 36 hours. GP96 was labeled with anti-GP96 and Alexa Fluor 488-conjugated antibodies, while
571 integrin α_V was labeled with anti-integrin α_V and Alexa Fluor 594-conjugated antibodies. DAPI
572 was used to stain DNA in the nucleus. **c**, **d**, A549 cells were infected with IAV for 36 hours.
573 Following washing steps, they were incubated with an antibody against integrin α_V (**c**) or RGD
574 peptide (**d**) for one hour, then IAV-infected cells were coinfected with an *S.pneumoniae* strain at
575 an MOI of 5. At two hours after initiating infection, cells were lysed and cell-associated bacteria
576 recovered. Bacterial adherence rate was calculated as percent of inoculum. All experiments were
577 performed in sextuplet with three technical repeats. Values are shown as the mean ± S.D. of six
578 wells from a representative experiment. **P* <0.01.
579
580 **Fig. 4. Calpain and Snail1 related to destruction of alveolar epithelial barrier following IAV**
581 **infection.**

582 **a**, A549 cells were infected with IAV for 1 hour. After transferring to fresh medium, incubation
583 was continued for 36 hours. GP96 was labeled with anti-GP96 and Alexa Fluor 594-conjugated
584 antibodies, while calpains were labeled with anti-calpain 2 and Alexa Fluor 488-conjugated
585 antibodies. DAPI was used to stain DNA in the nucleus. **b**, Transcriptional levels of genes
586 encoding junctional proteins and regulators in A549 cells infected with IAV were analyzed using
587 real-time RT-PCR. The *gapdh* transcript served as an internal control. Data from three
588 independent tests are presented, with values shown as the mean ± SD for expression ratio.
589 Transcriptional levels of tested genes are presented as relative expression levels normalized to
590 that of non-infected cells. **P* <0.01. **c**, A549 cells were infected with IAV for one hour, then
591 incubated with fresh medium in the presence or absence of SB-431542. Following washing steps,
592 cells were infected with an *S. pneumoniae* strain for seven hours. Expressions of E-cadherin,
593 p120-catenin, and Snail1 were detected in whole cell lysates using Western blot analysis. β-actin
594 served as a loading control.
595
596 **Fig. 5. GP96 a crucial factor for exacerbation of bacterial pneumonia following IAV**
597 **infection.**
598 **a**, Schematic showing experimental design. Mice were intranasally infected with IAV (day 0),
599 followed by *S. pneumoniae* on day 6. In some experiments, PU-WS13, a GP96 inhibitor, was

600 intratracheally administered. **b**, Effect of PU-WS13 treatment on bacterial burden in lungs. Values
601 shown represent the mean ± S.D. of quintuplet samples and are representative of at least three
602 independent experiments. **P* <0.01. **c**, **d**, Transcriptional levels of genes encoding GP96 and
603 integrin β_6 in pharyngeal (**c**) and lung tissues (**d**) infected with IAV- and *S. pneumoniae* were
604 analyzed by real-time RT-PCR. The *gapdh* transcript served as an internal control. Values from
605 three independent tests are presented as the mean ± SD for expression ratio. **P* <0.01. **e**, Lung
606 tissues obtained from mice infected under various conditions were subjected to hematoxylin and
607 eosin staining. Boxed area is magnified and shown in lower panel. **f**, Transcriptional levels of E-
608 cadherin gene in lung tissues infected under various conditions were analyzed by real-time RT-
609 PCR. The *gapdh* transcript served as an internal control. Values from three independent tests are
610 shown as the mean ± SD for expression ratio. Transcriptional levels are presented as relative
611 expression levels normalized to that of non-infected tissues (**c**, **d**, **f**). **P* <0.01.
612

613 **References**

614 1. Morens, D. M., Taubenberger, J. K. & Fauci, A. S.
615 Predominant role of bacterial pneumonia as a cause of death in pandemic influenza:
616 implications for pandemic influenza preparedness. *J. Infect. Dis*. **198**, 962-970 (2008).
617 2. Joseph, C., Togawa, Y. & Shindo, N. Bacterial and viral infections associated with influenza.
618 *Influenza Other Respir. Viruses.* **7** (Suppl. 2), 105-113 (2013).
619 3. Metzger, D. W. & Sun, K. Immune dysfunction and bacterial coinfections following
620 influenza. *J. Immunol.* **191**, 2047-2052 (2013).
621 4. McCullers J. M. The co-pathogenesis of influenza viruses with bacteria in the lung. *Nat. Rev.*
622 *Microbiol*. **12**, 252-262 (2014).
623 5. Ganesan, S., Comstock, A. T. & Sajjan, U. S. Barrier function of airway tract epithelium.
624 *Tissue Barriers* **1**, e24997 (2013).
625 6. Matrosovich, M. N., Matrosovich, T. Y., Gray, T., Roberts, N. A. & Klenk, H. D.
626 Human and avian influenza viruses target different cell types in cultures of human airway
627 epithelium. *Proc. Natl. Acad. Sci. U. S. A.* **101**, 4620-4624 (2004).
628 7. McCullers, J. A. & Bartmess, K. C. Role of neuraminidase in lethal synergism between
629 influenza virus and *Streptococcus pneumoniae*. *J. Infect. Dis.* **187**, 1000-1009 (2003).
630 8. van der Sluijs, K. F. et al. Involvement of the platelet-

activating factor receptor in host defense against *Streptococcus pneumoniae* during postinfluenza pneumonia. *Am. J. Physiol. Lung Cell. Mol. Physiol.* **290**, L194-199 (2006).

9. McCullers, J. A. & Rehg, J. E. Lethal synergism between influenza virus and *Streptococcus pneumoniae*: characterization of a mouse model and the role of platelet-activating factor receptor. *J. Infect. Dis.* **186**, 341-350 (2002).

10. McCullers, J. A., Iverson, A. R. McKeon, R. & Murray, P. J. The platelet activating factor receptor is not required for exacerbation of bacterial pneumonia following influenza. *Scand. J. Infect. Dis.* **40**, 11-17 (2008).

11. Short, K. R. et al. Influenza virus damages the alveolar barrier by disrupting epithelial cell tight junctions. *Eur. Respir. J.* **47**, 954-966 (2016).

12. Golebiewski, L., Liu, H., Javier, R. T. & Rice, A. P. The avian influenza virus NS1 ESEV PDZ binding motif associates with Dlg1 and Scribble to disrupt cellular tight junctions. *J. Virol*. **85**, 10639-10648 (2011).

13. Marzec, M., Eletto, D. & Argon, Y. GRP94: An HSP90-like protein specialized for protein folding and quality control in the endoplasmic reticulum. *Biochem. Biophys. Acta.* **1823**, 774-787 (2012).

14. Cabanes, D. et al. Gp96 is a receptor for a novel *Listeria monocytogenes* virulence factor, Vip, a surface protein. *EMBO J.* **24**, 2827-2838 (2005).

649 15. Rechner, C., Kühlewein, C., Müller, A., Schild, H. & Rudel, T. Host
650 glycoprotein Gp96 and scavenger receptor SREC interact with PorB of disseminating
651 *Neisseria gonorrhoeae* in an epithelial invasion pathway. *Cell Host Microbe* **2**, 393-403
652 (2007).
653 16. Kerr, A. R. et al. The Ami-AliA/AliB permease of Streptococcus pneumoniae is involved in
654 nasopharyngeal colonization but not in invasive disease. *Infect. Immun.* **72**, 3902-3906 (2004).
655 17. Randow, F. & Seed, B. Endoplasmic reticulum chaperone gp96 is required
656 for innate immunity but not cell viability. *Nat. Cell. Biol.* **3**, 891-896 (2001).
657 18. Sinha, B. et al. Fibronectin-binding protein acts as *Staphylococcus aureus* invasin
658 via fibronectin bridging to integrin $\alpha_5\beta_1$. *Cell. Microbiol.* **1**, 101-117 (1999).
659 19. Fink, D. L., Green, B. A. & St Geme, J. W. 3rd.
660 The *Haemophilus influenzae* Hap autotransporter binds to fibronectin, laminin, and collagen
661 IV. *Infect. Immun.* **70**, 4902-4907 (2002).
662 20. Pracht, D. et al. PavA of *Streptococcus pneumoniae* modulates adherence, invasion, and
663 meningeal inflammation. *Infect. Immun.* **73**, 2680-2689 (2005).
664 21. Yamaguchi, M., Terao, Y. & Kawabata, S. Pleiotropic virulence factor - *Streptococcus*
665 *pyogenes* fibronectin-binding proteins. *Cell. Microbiol.* **15**, 503-511 (2013).
666 22. Ueda, M. et al. Highly pathogenic H5N1 avian influenza virus induces extracellular Ca2+

667 influx, leading to apoptosis in avian cells. *J. Virol.* **84**, 3068-3078 (2010).

668 23. Fujioka, Y. et al. A Ca^{2+}-dependent Signalling Circuit Regulates Influenza A Virus
669 Internalization and Infection. *Nat. Commun.* **4**, 2763 (2013).

670 24. Chun, J. & Prince, A. TLR2-induced calpain cleavage of epithelial junctional proteins
671 facilitates leukocyte transmigration. *Cell. Host. Microbe.* **5**, 47-58 (2009).

672 25. Shao, H. et al. Spatial localization of m-calpain to the plasma membrane by phosphoinositide
673 biphosphate binding during epidermal growth factor receptor-mediated activation. *Mol. Cell.*
674 *Biol.* **26**, 5481-5496 (2006).

675 26. Ikenouchi, J., Matsuda, M., Furuse, M. & Tsukita, S. Regulation of tight junctions during the
676 epithelium-mesenchyme transition: direct repression of the gene expression of
677 claudins/occludin by Snail. *J. Cell. Sci.* **116**, 1959-1967 (2003).

678 27. Ohkubo, T. & Ozawa, M. The transcription factor Snail downregulates the tight junction
679 components independently of E-cadherin downregulation. *J. Cell. Sci.* **117**, 1675-1685 (2004).

680 28. Nieto, M. A. The snail superfamily of zinc-finger transcription factors. *Nat. Rev. Cell. Biol.* **3**,
681 155-166 (2002).

682 29. Meliopoulos, V. A. et al. An Epithelial Integrin Regulates the Amplitude of
683 Protective Lung Interferon Responses against Multiple Respiratory Pathogens. *PLoS Pathog.*
684 **12**, e1005804 (2016).

30. Maruvada, R., Argon, Y. & Prasadarao, N. V. *Escherichia coli* interaction with human brain microvascular endothelial cells induces signal transducer and activator of transcription 3 association with the C-terminal domain of Ec-gp96, the outer membrane protein A receptor for invasion. *Cell. Microbiol.* **10**, 2326-2338 (2008).

31. Krishnan, S., Chen, S., Turcatel, G., Arditi, M. & Prasadarao, N. V. Regulation of Toll-like receptor 2 interaction with Ecgp96 controls *Escherichia coli* K1 invasion of brain endothelial cells. *Cell. Microbiol.* **15**, 63-81 (2013).

32. Lucas, R. et al. Protein kinase C-α and arginase I mediate pneumolysin-induced pulmonary endothelial hyperpermeability. *Am. J. Respir. Cell. Mol. Biol.* **47**, 445-453 (2012).

33. Mesquita, F. S. et al. Endoplasmic reticulum chaperone Gp96 controls actomyosin dynamics and protects against pore-forming toxins. *EMBO Rep.* **18**, 303-318 (2017).

34. Hammerschmidt, S. Adherence molecules of pathogenic pneumococci. *Curr. Opin. Microbiol.* **9**, 12-20 (2006).

35. Valle, J. et al. Bap, a biofilm matrix protein of *Staphylococcus aureus* prevents cellular internalization through binding to GP96 host receptor. *PLoS Pathog.* **8**, e1002843 (2012).

36. Na, X., Kim, H., Moyer, M. P., Pothoulakis, C. & LaMont, J. T. gp96 is a human colonocyte plasma membrane binding protein for *Clostridium difficile* toxin A. *Infect. Immun.* **76**, 2862-2871 (2008).

703 37. Li, N. et al. Influenza viral neuraminidase primes bacterial coinfection through TGF-β-
704 mediated expression of host cell receptors. *Proc. Natl. Acad. Sci. USA.* **112**, 238-243 (2015).
705 38. Wang, B., Li, S., Southern, P. J. & Cleary, P. P. Streptococcal modulation of cellular invasion
706 via TGF-β1 signaling. *Proc. Natl. Acad. Sci. USA.* **103**, 2380-2385 (2015).
707 39. Okamoto, S. et al. The *Streptococcus pyogenes* capsule is required for adhesion of bacteria
708 to virus-infected alveolar epithelial cells and lethal bacterial-viral superinfection. *Infect.*
709 *Immun.* **72**, 6068-6075 (2004).
710 40. Zhang, Y. et al. GP96 is a GARP chaperone and controls regulatory T cell functions. *J. Clin.*
711 *Invest.* **125**, 859-869 (2015).
712 41. Gratz, N. et al. Pneumococcal neuraminidase activates TGF-β signalling. *Microbiology* **163**,
713 1198-1207 (2017).
714 42. Clarke, T. B., Francella, N., Huegel, A. & Weiser, J. N. Invasive bacterial pathogens
715 exploit TLR-mediated downregulation of tight junction components to facilitate translocation
716 across the epithelium. *Cell Host Microbe* **9**, 404-414 (2011).
717 43. Shahangian, A. et al. Type I IFNs mediate development of postinfluenza bacterial pneumonia
718 in mice. *J. Clin. Invest.* **119**, 1910-1920 (2009).
719 44. Radsak, M. P. et al. The heat shock protein Gp96 binds to human neutrophils and monocytes
720 and stimulates effector functions. *Blood* **101**, 2810-2815 (2003).

721 45. Ran, F. A. et al. Genome engineering using the CRISPR-Cas9 system. *Nat. Protoc.* **8**, 2281-
722 2308 (2013).
723 46. Sumitomo, T., Nakata, M., Yamaguchi, M., Terao, Y. & Kawabata, S. S-
724 carboxymethylcysteine inhibits adherence of *Streptococcus pneumoniae* to human alveolar
725 epithelial cells. *J. Med. Microbiol.* **61**, 101-108 (2012).
726 47. Nakata, M. et al. Assembly mechanism of FCT region type 1 pili in serotype M6
727 *Streptococcus pyogenes*. *J. Biol. Chem.* **286**, 37566-37577 (2011).
728 48. Sumitomo, T., Nakata, M., Higashino, M., Yamaguchi, M. & Kawabata, S. Group A
729 *Streptococcus* exploits human plasminogen for bacterial translocation across epithelial barrier
730 via tricellular tight junctions. *Sci. Rep.* **6**, 20069 (2016).
731 49. Sumitomo, T. et al. Streptolysin S contributes to group A streptococcal translocation across
732 an epithelial barrier. *J. Biol. Chem.* **286**, 2750-2761 (2011).
733

734 **Acknowledgements**

735 This work was supported by AMED (grant number JP19fm0208007), and grants from JSPS

736 KAKENHI (JP19H03825, JP18K19643, JP17K11610, JP17H04369, JP17K19751, JP17H05103,

737 JP18K17027), as well as a GSK Japan Research Grant and the Takeda Science Foundation,

738 Kobayashi International Scholarship Foundation, and Naito Foundation. We thank A. Bando for

739 the helpful technical assistance.

740

741 **Authors' contributions**

742 T.S. and S.K. conceived and designed the experiments. T.S., M.N., S. N., Y. T., M.H.O., and Y.M.

743 performed the experiments. T.S., M.N., M.Y., and S.O. analyzed the data. T.S. and M.N.

744 contributed to writing of the manuscript. All authors participated in discussions related to the

745 present research, and reviewed and approved the final version of the manuscript.

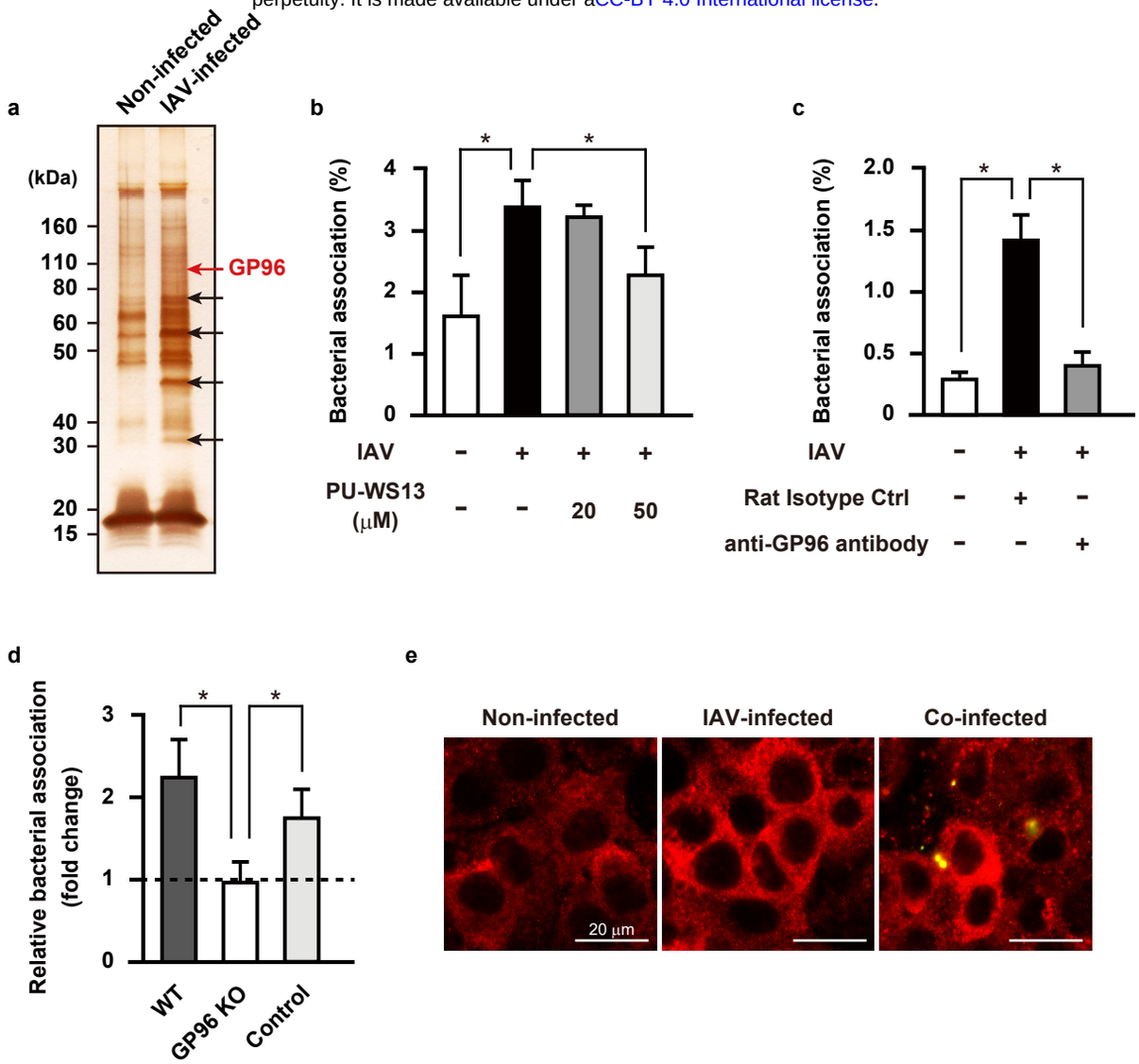

Fig. 1. IAV infection-induced surface display of GP96 promotes pneumococcal adherence.

a, A549 cells were infected with 10^6 PFU of IAV for 36 hours, then treated with a membrane-impermeable biotinylation regent. Cell surface proteins were obtained using streptavidin beads, then subjected to SDS-PAGE and silver staining. Arrows indicate bands of upregulated surface proteins after IAV infection. **b**, **c**, A549 cells were infected with IAV for one hour. Following washing steps, they were incubated for 36 hours in the presence of PU-WS13 (b) or an antibody against GP96 (c). Next, IAV-infected cells were coinfected with *S.pneumoniae* D39 strain at an MOI of 5. At two hours after infection, cells were lysed and cell-associated bacteria were recovered. Bacterial adherence rate was calculated as percent of the inoculum. All experiments were performed in sextuplet with three technical repeats. Values are shown as the mean ± S.D. of six wells from a representative experiment. **d**, Effect of GP96 knockout on pneumococcal adherence. Bacterial association with IAV-infected cells was normalized to that with non-infected cells. All experiments were performed in sextuplet with three technical repeats. Values are shown as the mean ± S.D. of six wells from a representative experiment. **P* <0.01 (b-d). **e**, A549 cells were infected with IAV followed by *S. pneumoniae* infection. GP96 was labeled with anti-GP96 and Alexa Fluor 594-conjugated antibodies (shown as red in images), while *S. pneumoniae* was labeled with anti-serotype 2 capsule and Alexa Fluor 488-conjugated antibodies (shown as green in images). Images were analyzed using a confocal laser scanning microscope. Values shown are representative of at least three separate experiments.

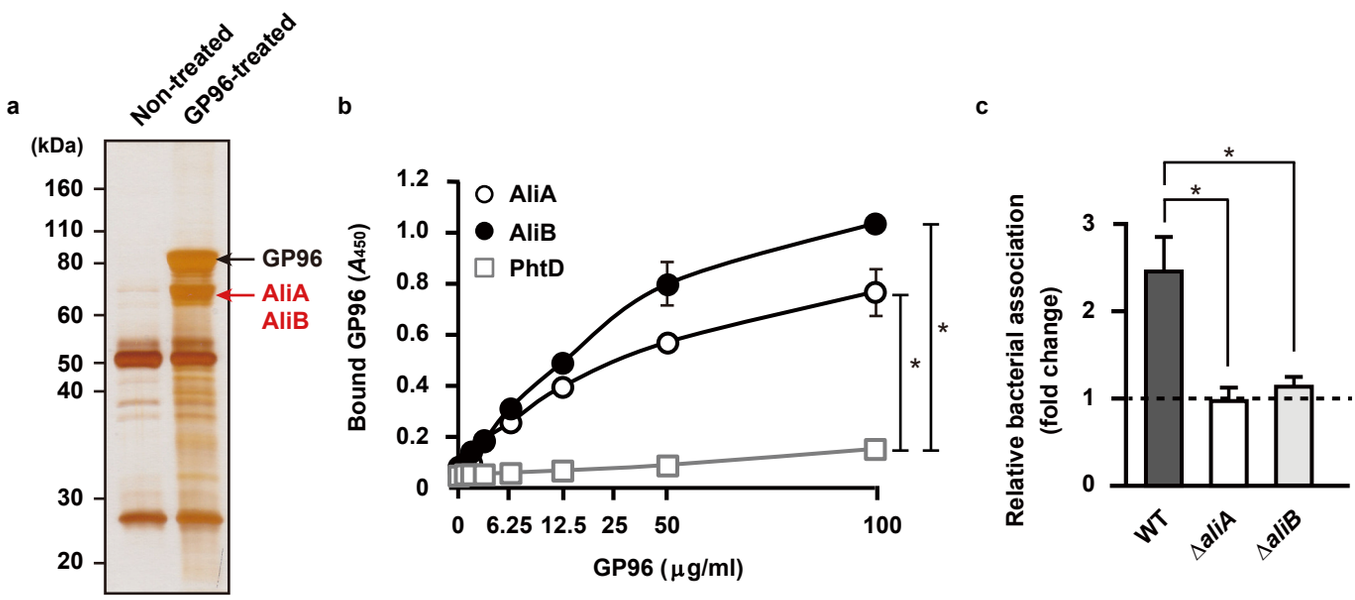

Fig. 2. *S. pneumoniae* adheres to alveolar epithelial cells through interaction of pneumococcal surface proteins with GP96.

a, Proteins bound to GP96 were immunoprecipitated from pneumococcal cell wall fractions, then subjected to SDS-PAGE and silver staining. **b**, AliA, AliB, and PhtD, bacterial surface proteins, were immobilized on microtiter plates, then increasing amounts of GP96 were added. Bound GP96 was detected using an anti-GP96 antibody. All experiments were performed in sextuplet with three technical repeats. Values are shown as the mean ± S.D. of six wells from a representative experiment. **P* <0.01. **c**, Effects of deletion of *aliA* and *aliB* on pneumococcal adherence. Bacterial association with IAV-infected cells was normalized to that with non-infected cells. All experiments were performed in sextuplet with three technical repeats. Values are shown as the mean ± S.D. of six wells from a representative experiment. **P* <0.01.

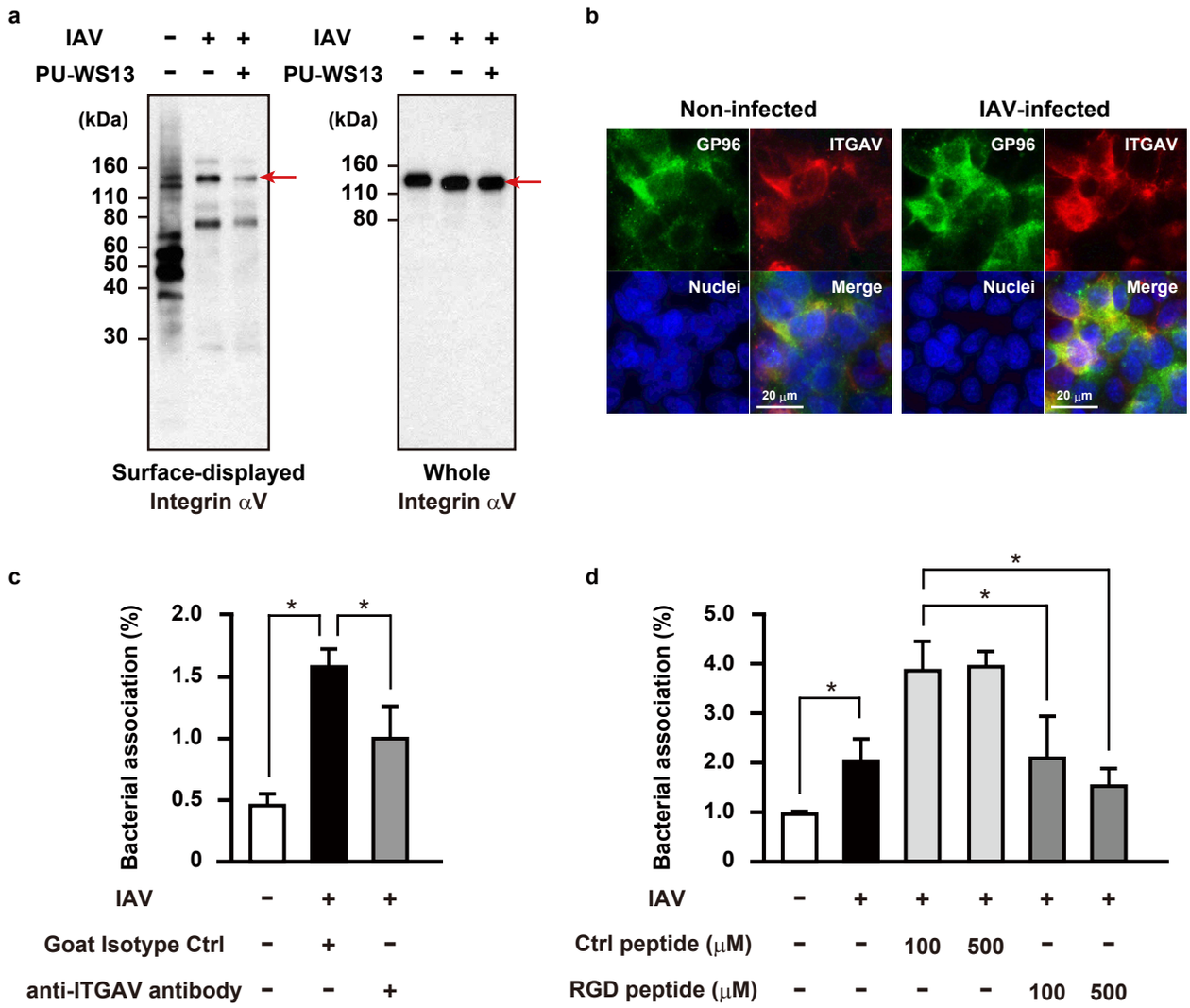

Fig. 3. GP96-dependent surface display of integrin α_v associated with enhanced pneumococcal adherence following IAV infection.

a, A549 cells were infected with IAV for 36 hours in the presence or absence of PU-WS13, then treated with a membrane-impermeable biotinylation reagent. Immunoprecipitation of cell lysates containing biotinylated surface proteins was performed using an antibody against integrin α_v. Surface-displayed and whole-cell integrin α_v was detected using streptavidin and an antibody against integrin α_v, respectively. Red arrows indicate integrin α_v band. **b**, A549 cells were infected with IAV for one hour. After transferring to fresh medium, incubation was continued for 36 hours. GP96 was labeled with anti-GP96 and Alexa Fluor 488-conjugated antibodies, while integrin α_v was labeled with anti-integrin α_v and Alexa Fluor 594-conjugated antibodies. DAPI was used to stain DNA in the nucleus. **c**, **d**, A549 cells were infected with IAV for 36 hours. Following washing steps, they were incubated with an antibody against integrin α_v (c) or RGD peptide (d) for one hour, then IAV-infected cells were coinfected with an *S.pneumoniae* strain at an MOI of 5. At two hours after initiating infection, cells were lysed and cell-associated bacteria recovered. Bacterial adherence rate was calculated as percent of inoculum. All experiments were performed in sextuplet with three technical repeats. Values are shown as the mean ± S.D. of six wells from a representative experiment. *P <0.01.

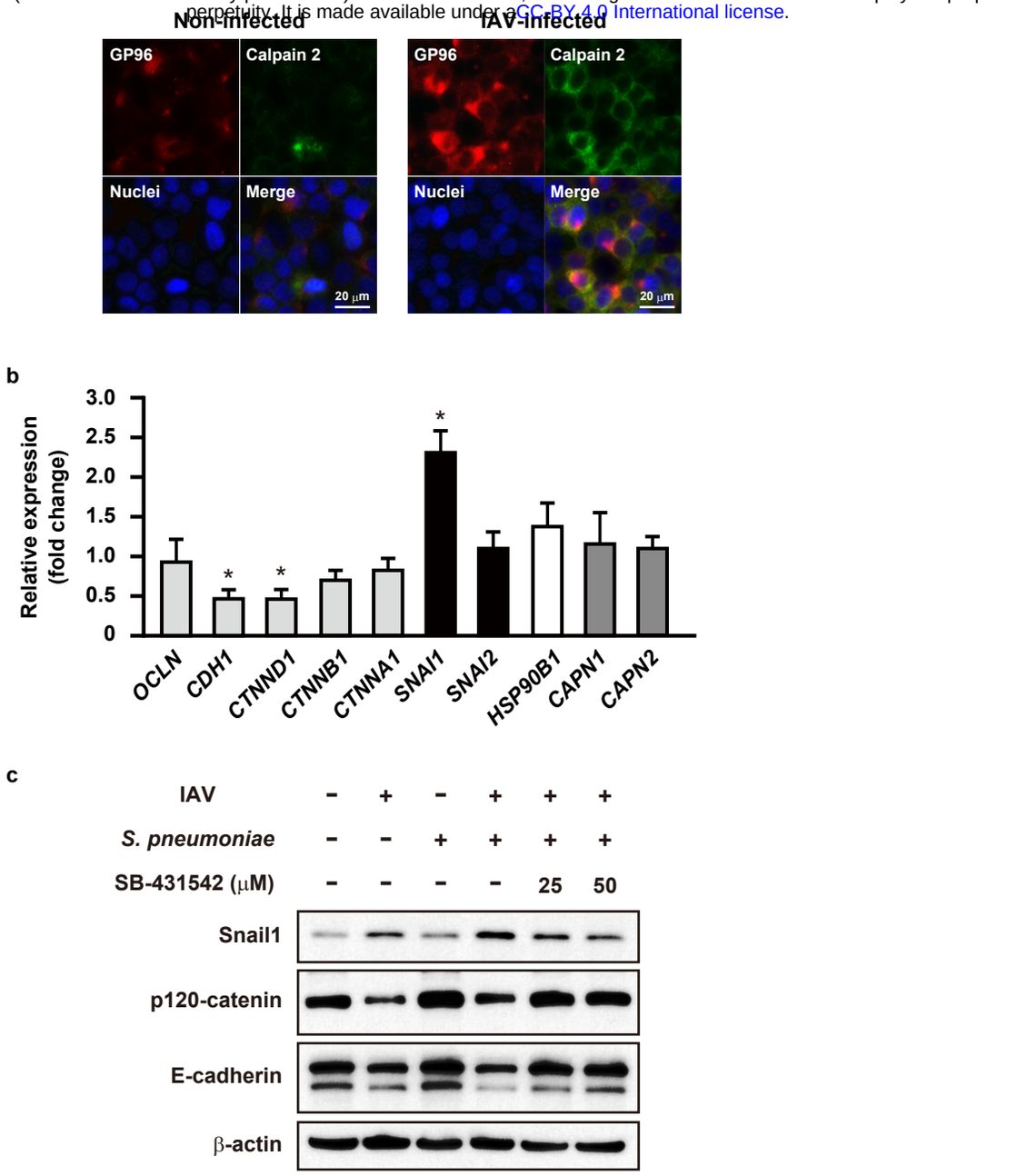

Fig. 4. Calpain and Snail1 related to destruction of alveolar epithelial barrier following IAV infection.

a, A549 cells were infected with IAV for 1 hour. After transferring to fresh medium, incubation was continued for 36 hours. GP96 was labeled with anti-GP96 and Alexa Fluor 594-conjugated antibodies, while calpains were labeled with anti-calpain 2 and Alexa Fluor 488-conjugated antibodies. DAPI was used to stain DNA in the nucleus. **b**, Transcriptional levels of genes encoding junctional proteins and regulators in A549 cells infected with IAV were analyzed using real-time RT-PCR. The *gapdh* transcript served as an internal control. Data from three independent tests are presented, with values shown as the mean ± SD for expression ratio. Transcriptional levels of tested genes are presented as relative expression levels normalized to that of non-infected cells. **P* <0.01. **c**, A549 cells were infected with IAV for one hour, then incubated with fresh medium in the presence or absence of SB-431542. Following washing steps, cells were infected with an *S. pneumoniae* strain for seven hours. Expressions of E-cadherin, p120-catenin, and Snail1 were detected in whole cell lysates using Western blot analysis. β-actin served as a loading control.

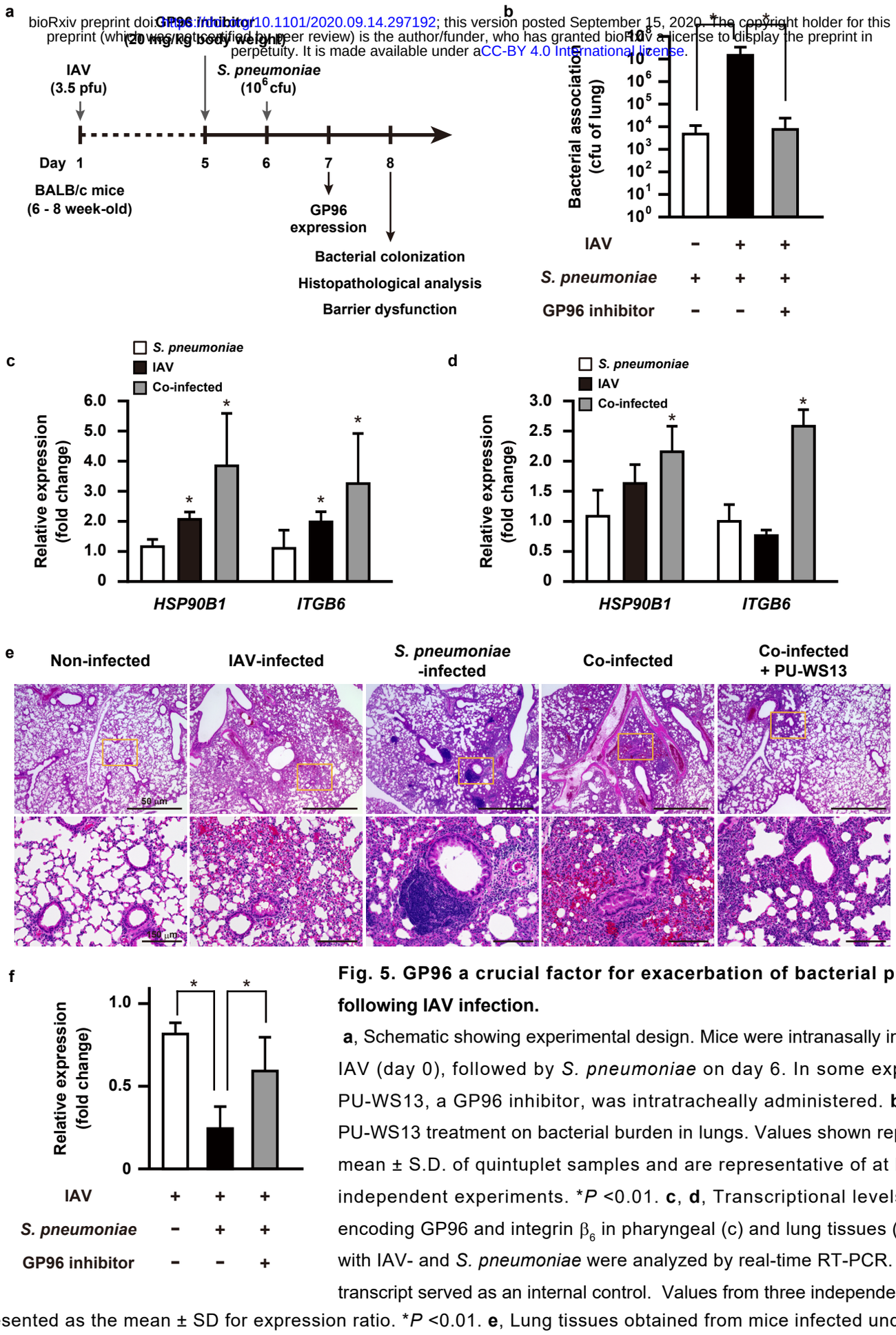

Fig. 5. GP96 a crucial factor for exacerbation of bacterial pneumonia following IAV infection.

a, Schematic showing experimental design. Mice were intranasally infected with IAV (day 0), followed by *S. pneumoniae* on day 6. In some experiments, PU-WS13, a GP96 inhibitor, was intratracheally administered. **b**, Effect of PU-WS13 treatment on bacterial burden in lungs. Values shown represent the mean ± S.D. of quintuplet samples and are representative of at least three independent experiments. **P* <0.01. **c**, **d**, Transcriptional levels of genes encoding GP96 and integrin β_6 in pharyngeal (c) and lung tissues (d) infected with IAV- and *S. pneumoniae* were analyzed by real-time RT-PCR. The *gapdh* transcript served as an internal control. Values from three independent tests are presented as the mean ± SD for expression ratio. **P* <0.01. **e**, Lung tissues obtained from mice infected under various conditions were subjected to hematoxylin and eosin staining. Boxed area is magnified and shown in lower panel. **f**, Transcriptional levels of E-cadherin gene in lung tissues infected under various conditions were analyzed by real-time RT-PCR. The *gapdh* transcript served as an internal control. Values from three independent tests are shown as the mean ± SD for expression ratio. Transcriptional levels are presented as relative expression levels normalized to that of non-infected tissues (c, d, f). **P* <0.01.

Table 1 Kinetic binding parameters for pneumococcal surface protein to GP96

Ligand	k_a (M^{-1} s^{-1})	k_d (s^{-1})	K_D (M)
AliA	2.31×10^{4}	7.85×10^{-4}	3.40×10^{-8}
AliB	2.09×10^{8}	10.12	4.85×10^{-8}

Sumitomo *et al.* Supplemental table 1

Table S1. Oligonucleotides used in this study.

Primer	Sequence (5'-3')	Purpose
gp96koF	CACCGTCATTCTGTTAACTTCGGCT	deletion of the *gp96* gene
gp96koR	AAACAGCCGAAGTTAACAGAATGAC	deletion of the *gp96* gene
gp96checkF	ACTTTGCTTTTTAGTAGAGGAA	confirmation of the *gp96* deletion
gp96checkR	TTACTTTTGCAGTAAATTAAG	confirmation of the *gp96* deletion
aliAkoF1	TTACGCTTTACCATCATGATCAGC	deletion of the *aliA* gene
aliAkoR1	CTTTATTAATTTGTTCGTATGTATTCATCATTTTCTCCTTTAAAACTTTCTCTCC	deletion of the *aliA* gene
aliAkoF2	GGAGAGAAAGTTTTAAAGGAGAAAATGATGAATACATACGAACAAATTAATAAAG	deletion of the *aliA* gene
aliAkoR2	CTAAATCCTTTCTTATATTTTGCAACAGTTATAATTTTTTTAATCTGTTATTTAAATAG	deletion of the *aliA* gene
aliAkoF3	CTATTTAAATAACAGATTAAAAAAATTATAACTGTTGCAAAATATAAGAAAGGATTTAG	deletion of the *aliA* gene
aliAkoR3	ACGACTACCTCTATACCAAGTGC	deletion of the *aliA* gene
aliAkockF	GTTAGAACAACCTCTTCTTCATGC	confirmation of the *aliA* deletion
aliAkockR	ACTGTGTCAAAGAGATTGACATCG	confirmation of the *aliA* deletion
aliBkoF1	CCGATAACCCCCATAGGTTAGC	deletion of the *aliB* gene
aliBkoR2	CTATTTAAATAACAGATTAAAAAAATTATAAAATCTAATTGTAGATAAGTTTGTGTAAG	deletion of the *aliB* gene
aliBkoF2	CTTACACAAACTTATCTACAATTAGATTTTATAATTTTTTTAATCTGTTATTTAAATAG	deletion of the *aliB* gene
aliBkoR2	CAAATATTTAAAGCAGGAGGTTCTGGAAATGAATACATACGAACAAATTAATAAAG	deletion of the *aliB* gene
aliBkoF3	CTTTATTAATTTGTTCGTATGTATTCATTTCCAGAACCTCCTGCTTTAAATATTTG	deletion of the *aliB* gene
aliBkoR3	TCAGCCAATCCTAATAAAATCACG	deletion of the *aliB* gene
aliBkockF	CTAGAATAAACAGTTACAAAATTAGC	confirmation of the *aliB* deletion
aliBkockR	GCTCTTCCAGATTTTGGATCAGC	confirmation of the *aliB* deletion
rGP96F	CGGGATCCGACGATGAAGTTGATGTGGATGGTAC	construction of rGP96
rGP96R	GCGTCGACCTTTGCATCAGGGTCAATGTTC	construction of rGP96
rAliAF	CGCGAGCTCAAAGGTGAGAAGACATTCTCATAC	construction of rAliA
rAliAR	ACGCGTCGACTTTCACATGTTTTGCGAGATCTTC	construction of rAliA
rAliBF	CGCGAGCTCAATTCTAGCACTGCATCAAAAACC	construction of rAliB
rAliBR	ACGCGTCGACTTTGACATGTTTTGCCAATTCTTC	construction of rAliB
OCLNF	CACACAGGACGTGCCTTCAC	real-time RT-PCR
OCLNR	GAGTATGCCATGGGACTGTCAA	real-time RT-PCR
CDH1F	CCAGTGAACAACGATGGCATT	real-time RT-PCR
CDH1R	TGCTGCTTGGCCTCAAAAT	real-time RT-PCR

CTNND1F	TGCACTGCATGCCTTGACA	real-time RT-PCR
CTNND1R	GTTCCCGCTCCCAACCA	real-time RT-PCR
CTNNB1F	TGCCATTCCACGACTAGTTCAG	real-time RT-PCR
CTNNB1R	CGTACGGCGCTGGGTATC	real-time RT-PCR
CTNNA1F	GAATGTCTGCAAGCCAGTTAGAAG	real-time RT-PCR
CTNNA1R	TGCTAAAGCCAGTGCAGCAT	real-time RT-PCR
SNAI1F	TTCAACTGCAAATACTGCAACAAG	real-time RT-PCR
SNAI1R	GCGTGTGGCTTCGGATGT	real-time RT-PCR
SNAI2F	ACGCCCAGCTACCCAATG	real-time RT-PCR
SNAI2R	TCACTCGCCCCAAAGATGAG	real-time RT-PCR
hHSP90B1F	GCCCCCTAATCCCCTTCTC	real-time RT-PCR
hHSP90B1R	CCACTTTTTCCTGTGACCCATAA	real-time RT-PCR
CAPN1F	CACGACACCCTGATCTGAAGAC	real-time RT-PCR
CAPN1R	CCACCATGCTGCGACATG	real-time RT-PCR
CAPN2F	CCTGCTGGAGAAGGCATACG	real-time RT-PCR
CAPN2R	GGCACCCCCTGATAGTGCTT	real-time RT-PCR
GAPDHF	CGGACTTCCTCGGTGATACC	real-time RT-PCR
GAPDHR	CAATGCCGGCCTTAGCAT	real-time RT-PCR
mHSP90B1F	GTCAAAAGAAAACGTTCGAAATCA	real-time RT-PCR
mHSP90B1R	CCGCCGCAACATGTCTCT	real-time RT-PCR
mITGB6F	AAGGCCAAGTGGCAAACG	real-time RT-PCR
mITGB6R	CGTTCTTAAAAGTGCTGGTGGAA	real-time RT-PCR
mCDH1F	ACCCCCTTACGACTCTCTGTTG	real-time RT-PCR
mCDH1R	CAGGCTAGCGGCTTCAGAAC	real-time RT-PCR
mGAPDHF	CATGGCCTTCCGTGTTCCTA	real-time RT-PCR
mGAPDHR	GCGGCACGTCAGATCCA	real-time RT-PCR